Quantum mechanical calculations of dioctahedral 2:1 phyllosilicates: Effect of octahedral cation distributions in pyrophyllite, illite, and smectite

C. Ignacio Sainz-Díaz,[1,*] Vicente Timón,[2] Vicente Botella,[2] Emilio Artacho,[3] and Alfonso Hernández-Laguna[1]

[1]Departamento de Ciencias de la Tierra y Química Ambiental, Estación Experimental del Zaidín (C.S.I.C.), C/Profesor Albareda,1, 18008 Granada, Spain
[2]Instituto de Estructura de la Materia (C.S.I.C.), C/Serrano 113, 28006 Madrid, Spain
[3]Department of Earth Sciences, University of Cambridge, Downing Street, Cambridge CB2 3EQ, U.K.

ABSTRACT

The structure of dioctahedral 2:1 phyllosilicates with different interlayer charge was studied theoretically using ab initio calculations. The standard Kohn-Sham self-consistent density functional method was used in the generalized gradient approximation (GGA), with numerical atomic orbitals as the basis set, by means of the SIESTA program. Once the method had been checked satisfactorily, the theoretical study was extended beyond the systems for which there are experimental information, and structural characteristics were predicted. The SIESTA program was shown to be a useful tool in studying the crystallographic properties of 2:1-dioctahedral phyllosilicates. The crystal structures of pyrophyllite, beidellite, and other smectites and illites were simulated. The experimental crystallographic properties of phyllosilicates with high, medium, and low interlayer charge were reproduced. The calculated structures agree with the main experimental structural features of the crystal lattice of these minerals. The effect of cation substitutions in the octahedral and tetrahedral sheets was also studied. The calculated effects are consistent with experimental results. The Mg^{2+} cations were found to have a tendency to be distributed in the octahedral sheet, in contrast to Fe^{3+} ions that tend to be clustered.

INTRODUCTION

The 2:1 phyllosilicate clay minerals share the common structural feature of single sheets of octahedrally coordinated cations sandwiched between two layers of tetrahedra. The great diversity of these layered silicates is due to isomorphous substitution of various cations in the octahedral and tetrahedral sheets. These substitutions include Al^{3+} by Mg^{2+}, Fe^{3+}, and Fe^{2+} in the octahedral sheet, and Si^{4+} by Al^{3+} in the tetrahedral sheet, and can result in a net negative charge of the layers. This charge is compensated by the presence of additional cations in the interlayer space. In this space, the cations can be exchanged easily. Organic or water molecules can intercalate between the layers, inducing swelling of the clays (Karaborni et al. 1996). The geometric similarity of the layers of these minerals facilitates the formation of structures containing different kinds of layers and in different arrangements, ordered and disordered. Cation substitutions (in the octahedral and tetrahedral sheets) also give rise to disorder in these minerals. All these types of structural disorder and the small size of the crystals in clays make it difficult to obtain good experimental structural data by means of X-ray, neutron, or electron diffraction techniques, especially in the case of smectites and illites. The valuable catalytic and adsorptive properties of clays demand a firm theoretical understanding of their structure and behavior. Our understanding of some of the important issues in the experimental behavior of these minerals is aided by the application of theoretical studies. Such issues include mineral transformations, chemical transport in the environment and some industrial applications of clays, in catalysis, and as a barrier component for nuclear waste and other pollutant deposits.

The cation distribution in the tetrahedral sheet of micas has been studied experimentally and theoretically (Herrero and Sanz 1991; Palin et al. 2001). These authors found a random distribution of cations in the tetrahedral sheet with the Loewenstein rule of AlAl pair avoidance. Reverse Monte Carlo simulations have been used to study the octahedral cation distribution in illite-smectite systems taking into account experimental NMR and IR spectra (Cuadros et al. 1999; Sainz-Diaz et al. 2001a). A short-range ordering in the Fe and Mg distribution was found in these studies.

Much effort has been dedicated to the modeling of mineral structures at the atomic level, thanks to the important advances in theory and computer technology in recent years (Lasaga 1995; Sauer et al. 1994). Modeling of layered phyllosilicates with high interlayer charge, such as muscovite, has been reported, where models of empirical interatomic potentials were applied (Collins and Catlow 1992; Bosenick et al. 2001). However, clay structures with low interlayer charge are difficult to treat using empirical potentials. In general, these methods describe reasonably well the experimental crystal lattice structure of clays (Teppen et al. 1997; Sainz-Diaz et al. 2001b). However, some geometrical features, such as the interlayer

spacing, are not well reproduced. Hydrogen bonding, low symmetry, and relatively weak interactions in the interlayer space require the more sophisticated and exact methods provided by quantum-mechanical calculations. Many approximations have been reported applying quantum-mechanical studies on clusters or molecular models of these infinite structures with interesting results (Lasaga 1995; Kubicki et al. 1996; Kubicki and Apitz 1998; Sainz-Diaz et al. 2000). First Principles quantum techniques, based on density functional theory (DFT) with periodic boundary conditions that avoid the edge effects associated with the cluster approach, have been used in the study of some minerals (Sherman 1991; Smrcok and Benco 1996; Winkler et al. 1995; 2001) including layered phyllosilicates (Bridgeman et al. 1996; Hobbs et al. 1997; Chatterjee et al. 2000).

One of the aims of this work is to find a suitable model for reproducing the experimental structure of phyllosilicates with low interlayer charge. We report on a wide range of 2:1 dioctahedral clays. In most cases, we are able to obtain reasonably good agreement with experimental data, and can account for trends in structural features with chemical composition. We are able to extend the range of calculations beyond the systems for which there are experimental data in order to predict the crystal structures of materials for which experimental structural data are difficult to obtain.

METHODS

Mineral models

Different models of dioctahedral 2:1 phyllosilicates with varying compositions were studied in this work (Table 1). This series tries to cover a wide range of tetrahedral, octahedral, and interlayer (IC) charges, including pyrophyllite (no significant IC), smectites (low IC, mainly from octahedral sheet), and illites (medium IC, mainly from tetrahedral sheet). Different interlayer cations were included (i.e., Na^+, K^+, Mg^{2+}, and Ca^{2+}). Different cation substitutions of Si^{4+} by Al^{3+} in the tetrahedral sheet, and Al^{3+} by Mg^{2+} and Fe^{3+} in the octahedra were included. In this series, there are samples with and without tetrahedral charge, and samples with and without octahedral charge.

TABLE 1. Chemical composition of the illite-smectite samples studied

Sample	Si^{4+} (T)	Al^{3+} (T)	Al^{3+} (Oc)	Mg^{2+} (Oc)	Fe^{3+} (Oc)	Interlayer cation
pyro	8		4			
S1	7	1	4			Na^+
S2	7	1	2		2	Na^+
S3	8		2	2		$2Na^+$
S4	8		3	1		Na^+
S5	8		2	1	1	Na^+
S6	7	1	3		1	Na^+
S7	7	1	4			K^+
S8	7	1	2		2	K^+
S9	8		2	2		$2K^+$
S10	8		3	1		K^+
S11	8		2	1	1	K^+
S12	7	1	3		1	K^+
S13	7	1	3	1		Mg^{2+}
S14	7	1	3	1		Ca^{2+}
S15	8		2		2	Ca^{2+}

Note: Structural formulae on the basis O_{20} (OH)$_4$ (T = tetrahedral, Oc = octahedral).

Samples with a high Fe content in the octahedral sheet have been also included.

The pyrophyllite experimental structural data were taken from X-ray diffraction studies (Lee and Guggenheim 1981; Wardle and Brindley 1972). In the smectite/illite samples, no experimental atomic co-ordinate set was available. Nevertheless, the initial geometries were taken from the models proposed by Tsipursky and Drits (1984) based on oblique-texture electron diffraction studies of dioctahedral smectites. The experimental hydrogen positions of pyrophyllite, smectites, and illites were taken from the Giese (1979) studies on pyrophyllite. These positions were optimized in a previous study (Sainz-Diaz et al. 2001b).

Theoretical methods

Total energy calculations based on DFT and pseudo-potentials were performed using the numerical atomic orbital (NAO) methodology (Ordejón et al. 1996) implemented in the SIESTA program (Artacho et al. 1999; Sánchez-Portal et al. 1997). This is a method that scales linearly with the number of atoms in the simulation cell. The generalized gradient approximation (GGA) was used because hydrogen-bonded systems are better described using gradient-corrected DFT (Lee et al. 1993). The Perdew-Burke-Ernzerhof parameterization of the exchange-correlation functional was employed (Perdew et al. 1996). A uniform mesh with certain plane-wave cut-off energy is used to represent the electron density, the local part of the pseudo-potential, and the Hartree and exchange-correlation potentials. Calculations were restricted to the Γ point in the Brillouin zone, because previous work (Stich et al. 1996) found cell-size effects to be small. In all structures, all atoms and all cell parameters were relaxed by means of conjugated gradient minimizations.

Core electrons were replaced by norm-conserving pseudo-potentials (Troullier and Martins 1991) factorized in the Kleinman-Bylander form (Kleinman and Bylander 1982), including scalar-relativistic effects (Bachelet and Schluter 1982), and nonlinear partial-core corrections (Louie et al. 1982) in some cases. The pseudo-potentials simulate the interaction between the valence electrons and the cores (nuclei plus core electrons) and neither core electrons nor core wave functions are necessary. With this approximation the valence wave functions are substituted by pseudo-wave functions that do not present strong oscillations in the core region. In the case of potassium, a partial core correction (Louie et al. 1982) was used, because it is necessary for alkali metal elements (Hebenstreit and Scheffler 1992). The same correction was applied for the iron atoms. Scalar relativistic effects were also included for the potassium and iron atoms. Illustrative is the fact that the c parameter and the β angle of the S7 system (see below) were badly reproduced without these corrections (11.92 Å and 100.69°, respectively, compared with experimental values of 10.10 Å and 101.4°, respectively). The inclusion of these corrections resulted in improved values of 10.39 Å and 101.77°.

Special care had to be taken with the pseudo-potential cut-off radii of K, due to its very wide atomic orbitals. In Figure 1 the pseudo-wave functions are compared with the all-electron wave functions for two different sets of radii (r_{c1} = 3.65, 3.75, and 3.75 bohrs, and r_{c2} = 3.10, 3.30, and 3.30 bohrs for the 4s,

4p, and 3d orbitals, respectively). We observe that the r_c is still higher than the outermost radial node and no significant oscillation was detected in the pseudo-wave functions (Fig. 1b). The former would seem to be the one of choice, but they show reduced transferability, which can be seen in the values of the c parameter and β angle of the S7 system (c = 10.39 Å, β = 101.77°), compared with experimental values (c = 10.10 Å, β = 101.4°), whereas the shorter radii offer better results (c = 10.18 Å, β = 101.31°, see below).

The wave functions describing the valence electrons were expanded in bases of atomic orbitals in a similar manner as with quantum-chemical methods. The basis sets used in this work were double-zeta (DZ), meaning that there are two orbitals of the same symmetry for each of the orbitals relevant to the description of the valence electrons in the corresponding isolated atoms. Polarization orbitals were used as well, meaning orbitals with a higher angular momentum than the free-atom orbitals. A double-zeta polarized (DZP) basis for the Si atom will thus have two 3s orbitals, two 3p shells, and one 3d shell polarizing the p orbital. The radial shape of the different orbitals was obtained from the solution of the isolated pseudo-atom problem. The polarization orbitals were obtained by applying a small external electric field to the same isolated pseudo-atom (Artacho et al. 1999).

There are two important differences with respect to usual quantum-chemical methods: (1) The radial shape of the orbitals is not bound to any analytical form, like gaussian or Slater-type, but tabulated numerically in a radial grid (numerical atomic orbitals, NAOs); and (2) they are strictly localized, meaning that the tail of every basis function strictly vanishes beyond a certain cutoff radius. The cutoff radius depends on the specific orbital and chemical species. The different radii are defined by choosing the excitation energy that every orbital must experience when constrained, the so-called energy shift (Artacho et al. 1999). This strict localization of the basis set allows the calculation of all the required matrix elements in linear-scaling operations. In this study the energy shift was 270 meV.

Some calculations in this study were performed with CASTEP for testing purposes, a method very similar to SIESTA in all respects except for the basis (CASTEP uses plane waves) and the linear-scaling properties.

RESULTS AND DISCUSSION

Previous theoretical studies of dioctahedral 2:1 phyllosilicates described quite well the crystal lattice structure by means of empirical potentials (Sainz-Diaz et al. 2001b). However, in some cases, the c parameter and interlayer space were not well described in layered silicates with no interlayer charge (pyrophyllite) or with very low interlayer charge, and in samples with divalent interlayer cations. First Principles calculations are thus needed for studying these minerals.

Pyrophyllite

The main geometrical features of the calculations for pyrophyllite are described in Table 2. The calculations with the DZP basis set reproduce the experimental data better than those with the DZ basis set. Hence the use of basis sets with polarization functions is necessary for reproducing experimental structural values. The use of a polarized basis increases the computational effort, however the high content of highly polarizable O atoms in these minerals makes necessary the use of polarized orbitals. Cut-off energy values should be at least 150 Ry to avoid convergence problems and to reproduce experimental structural values[1]. Calculations with cut-off energy of 250 and 350 Ry were performed with similar results to those with 150 Ry, although with much more computational effort.

Our calculated lattice parameters match the experimental values (Table 2). The experimental M-O and M-OH bond lengths (M = octahedral cation) are closely reproduced in these calculations. The theoretical T-O bond length (T = tetrahedral cation) is slightly longer than the experimental values, a problem that has been traced to the perturbative polarization orbitals of T (Junquera et al. 2001). The standard deviation of all parameters with respect to the experimental values is lower than 2%. This agreement is better than those previously obtained with empirical potential calculations (Teppen et al. 1997; Sainz-Diaz et al. 2001b), especially for the c parameter. Therefore, the total energy calculations at First Principles level de-
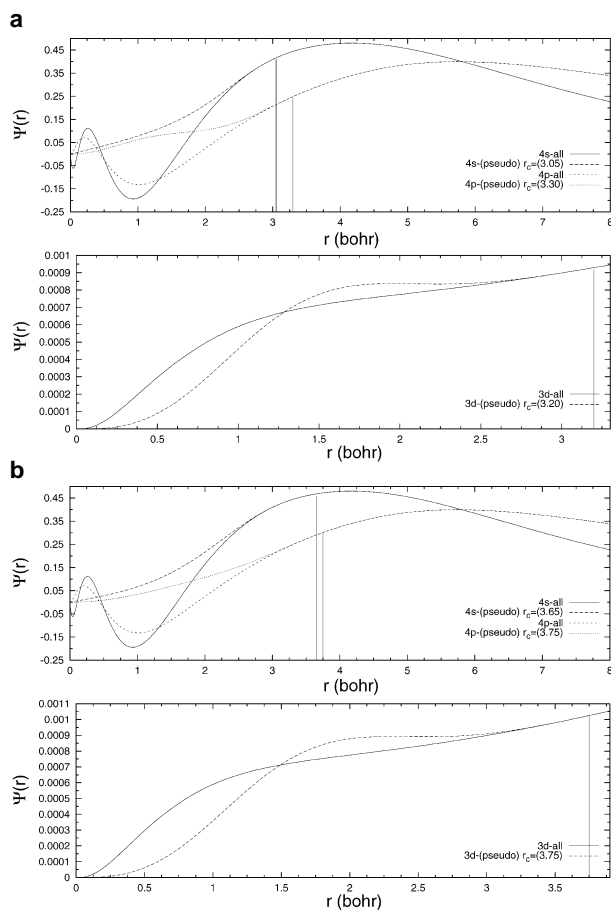

FIGURE 1. Graphical representations of the all-electron and pseudo-wave functions of the K atom (**a**) for r_c = 3.65 and 3.75 bohrs for the 4s and 4p orbitals, respectively, and (**b**) for r_c = 3.10 and 3.30 bohrs for the 4s and 4p orbitals, respectively.

TABLE 2. Experimental and calculated structural features of pyrophyllite (lengths in Å and angles in degrees)

Sample	Exp*	Calculated	
Basis set †		DZ	DZP
Cut-off (Ry) ‡		250	150
a	5.16	5.33	5.15
b	8.97	9.26	8.98
c	9.35	8.30	9.21
α	91.20	90.65	88.96
β	100.50	98.69	99.80
γ	89.60	90.42	90.0
V(Å^3)	425.60	405.44	420.23
Tetrahedral sheet thickness	2.15	–	2.17
Octahedral sheet thickness	2.08	–	2.13
Mean O-T-O §	109.50	–	110.1
ΔZ||	0.24	0.68	0.31
τ#	109.2		108.6
ψ**	57.0		56.7
Mean O-H	–		0.977
Mean T-O §	1.62		1.67
Mean M-O §	1.91 – 1.94		1.94
Mean M-OH §	1.89		1.90

* Experimental data of $(Si_{3.98}Al_{0.02})(Al_{1.97}Fe^{3+}_{0.03})O_{10}(OH)_2$ (Lee and Guggenheim 1981; Wardle and Brindley 1972).
† DZ: Double zeta basis set, DZP: DZ with polarization function on all atoms except H atoms.
‡ Mesh cut-off energy.
§ T is the cation of the tetrahedral sheet, M is the cation of the octahedral sheet.
|| Corrugation effect of basal surfaces.
τ is the O_{basal} - T-O_{apical} bond angle.
** Octahedral flattening angle, ψ, cos ψ = Oct. th. / 2(M-O)].

scribe properly the crystal structure of pyrophyllite including the interlayer space, where the interatomic interactions are very weak.

Illite-smectites (I-S)

In these systems, cation substitutions in the tetrahedral and octahedral sheets produce an interlayer negative charge that has to be compensated by the presence of interlayer cations. We studied the following aspects of this system: (1) The soft interactions in the interlayer space with respect to the interlayer cation, (2) the effect of the cation substitution on the crystallographic properties, and (3) the effect of the octahedral cation distribution in these minerals.

Our calculations reproduce the experimental crystallographic values of the main crystal lattice parameters of the I-S series (Table 3)[1]. The calculated values of the a parameter are slightly lower than the experimental values. The rest of the parameters (b, c, and β) compare well with the experimental values. Although no experimental data for the rest of the structural parameters for illites/smectites are available, we can compare our results with the experimental data of muscovite

(Guggenheim et al. 1987). The calculated T-O, M-O, and O-H bond lengths are slightly higher than those obtained experimentally. In general, the agreement with experimental values is better than in previous studies with empirical potential calculations (Sainz-Diaz et al. 2001b). This improvement is remarkable in samples with divalent interlayer cations, Mg^{2+} and Ca^{2+} (S13-S15). For testing purposes, sample S7 was also calculated and optimized by means of the CASTEP program (Payne at al. 1992), where the electronic wave function is expanded using a plane-wave basis set with an equivalent energy cut-off of 380 eV, with ultra-soft pseudo-potentials and gradient-corrected density functional theory by means of the graphical interface package *Cerius2*. The geometrical features are similar to those obtained with SIESTA, although the computational effort is substantially larger than with SIESTA. Therefore, the geometrical accuracy obtained with the SIESTA calculations is validated by the good agreement with experiment and by the high similarity with the CASTEP calculation results performed for one standard illite.

The effect of cation substitution on structure

The cation substitution effect on the lattice parameters is small in our systems and composition range. Some previous statistical studies on phyllosilicates were performed with experimental data for correlating the parameter b with the cation composition. However, no general equation for all dioctahedral 2:1 phyllosilicates has been obtained yet, due to the wide variation of natural samples (Brown and Brindley 1980). No example of this correlation was reported previously for smectites and illites. In this theoretical work, a slight decrease of b and c is observed with increasing Fe content (Table 3). A reduction in of c is detected with increasing Al^{IV} content (in the tetrahedral sheet) and also a slight decrease of c is observed with an increase in Mg content in the octahedral sheet. This effect has also been observed experimentally (Tsipursky and Drits 1984; Sainz-Diaz et al. 2001b). The increase in Al^{IV} and Mg^{2+} content produces an increase in the interlayer charge and thus larger attractive interactions with cations in the interlayer space, which lowers decreasing the c parameter. This effect is observed also in the interlayer thickness.

In these phyllosilicates, some distortions from an ideal tetrahedral or octahedral sheet can be seen. The tetrahedral sheet can reduce its lateral dimensions to compensate for the smaller size of the octahedral sheet. Alternatively, the octahedral sheet can expand its lateral dimensions to compensate partly for this misfit. One of the structural distortions is the corrugation effect (ΔZ) of the basal O atoms in the tetrahedral sheet. This distortion produces a tilting of the tetrahedra out of the (001) plane. Another distortion in these minerals is the thickening effect on the tetrahedra determined by the O_{basal}-T-O_{apical} bond angle (τ). The flattening effect of the octahedra is another distortion in these minerals, and it is determined by the ψ angle [cos ψ = Oct. th./2(M-O), where Oct. th. is the octahedral sheet thickness and M-O is the bond length of this bond in the octahedral sheet]. In general, no significant correlation was detected between ΔZ and the cation substitutions. Nevertheless, an increase of τ and ψ was observed with increasing Mg^{2+} content. The higher ionic radius of Mg pushes out the apical tetrahedral

---

[1]For a copy of the unit-cell parameters and atomic crystallographic coordinates of the optimized structure of pyrophyllite, S1, S3 (smectite and illite, respectively), described in Appendix 1, contact the Business Office of the Mineralogical Society of America (see inside front cover of recent issue) for price information. Deposit items may also be available on the American Mineralogist web site (http://www.minsocam.org or current web address).

TABLE 3. Calculated and experimental structural parameters of illite-smectites (lengths in Å and angles in degrees)

Sample	Exp *	S1	S2	S3	S4	S5	S6	S7†	S8	S9	S10	S11	S12	S13	S14	S15
a	5.18	5.12	5.14	5.12	5.12	5.13	5.13	5.12 (5.16)	5.12	5.16	5.13	5.11	5.10	5.03	5.15	5.15
b	8.97–9.01	9.06	9.01	9.12	9.05	9.00	9.02	9.06 (8.89)	8.98	9.08	9.05	8.98	9.00	8.99	9.09	9.03
c	10.05–10.2	10.10	10.01	10.08	10.01	10.04	10.08	10.18 (10.3)	9.95	10.05	10.06	9.89	9.98	9.51	9.97	9.94
β	99.6–101.4	101.2	101.9	101.2	101.9	102.2	101.8	101.6 (101.1)	101.9	100.9	101.2	101.4	101.8	98.7	101.6	101.0
V (Å³)		459.4	454.0	461.4	453.4	454.0	457.2	463.4	447.4	462.4	457.6	444.5	448.2	425.4	457.4	453.5
T. th. ‡	2.25§	2.25	2.24	2.26	2.26	2.28	2.23	2.22	2.24	2.32	2.30	2.28	2.23	2.25	2.29	2.31
Oc. th. ‡	2.08§	2.13	2.11	2.21	2.17	2.16	2.12	2.13	2.13	2.19	2.16	2.16	2.13	2.18	2.15	2.18
Int. th. ‡		3.28	3.21	3.16	3.15	3.15	3.29	3.41	3.13	3.04	3.11	2.98	3.18	2.73	3.04	2.96
ΔZ||		0.27	0.28	0.21	0.24	0.21	0.22	0.22	0.22	0.15	0.24	0.19	0.26	0.21	0.24	0.19
τ||		110.8	111.8	112.5	111.1	111.3	110.3	111.0	110.8	112.4	111.0	111.1	110.5	111.3	111.3	113.5
ψ||	57.1–57.3§	57.1	57.2	56.6	57.3	57.5	57.1	56.9	56.9	57.2	57.3	56.6	56.9	56.8	57.1	56.8
O-H ||	0.95§	0.979	0.991	0.978	0.978	0.986	0.985	0.979	0.992	0.981	0.978	0.986	0.984	0.978	0.977	0.981
T-O ||	1.64§	1.66	1.67	1.63	1.65	1.65	1.67	1.67	1.67	1.63	1.66	1.66	1.67	1.65	1.65	1.63
M-O ||	1.94§	1.96	1.95	2.01	2.01	2.01	1.95	1.95	1.95	2.02	2.00	1.96	1.95	1.99	1.98	1.99
M-OH ||		1.91	1.90	2.05	1.96	1.96	1.92	1.91	1.89	1.97	1.95	1.96	1.92	1.93	1.94	1.96

* Experimental values of ilite-smectites (Tsipursky and Drits 1984).
† Values in brackets were calculated with CASTEP.
‡ T. th. = tetrahedral sheet thickness, O. th. = octahedral sheet thickness, Int. th. = interlayer thickness.
§ Experimental data of muscovite (Guggenheim et al. 1987).
\|\| Mean values, ΔZ = corrugation effect of basal oxygen surfaces, τ = the O_{basal}-T-O_{apical} bond angle, ψ = octahedral flattening angle cos ψ = Oct. th. / 2(M-O), T is the cation of the tetrahedral sheet, M is the cation of the octahedral sheet.

oxygen atoms, increasing τ. These parameters that characterize the distortions of octahedral and tetrahedral sheets are reproduced by our quantum-mechanical calculations for pyrophyllite. This agreement validates the predictive application of the distortion parameters calculated for smectites and illites, which have not been determined experimentally.

Increasing Mg^{2+} content leads to increasing M-O and M-OH bond lengths due to the greater ionic radius of Mg^{2+} with respect to Al^{3+}. Increasing the Fe^{3+} content results in a greater O-H bond length. This increase is related with a decrease of the stretching vibrational frequency ν(OH). Hence, this is consistent with the experimental results of the cation substitution effect on ν(OH) in the octahedral sheet of illite-smectites, where the ν(OH) frequency decreases with increasing Fe content (Besson and Drits 1997). This effect has been also found by means of quantum-mechanical calculations on molecular clusters representing dioctahedral pairs in the octahedral sheet of these minerals (Sainz-Diaz et al. 2000).

Samples with Na^+ in the interlayer space showed similar cell parameters and T-O, M-O, and M-OH bond lengths relative to those with K^+. However, in spite of the higher ionic radius of K^+ with respect to Na^+, the samples with K^+ showed a slightly smaller c dimension than those with Na^+. Hence, our calculations reproduce the known experimental phenomenon that the potassium ion fits better into the hexagonal hole of the tetrahedral layer, decreasing the interlayer distance. This fact can be considered as the first step in the smectite to illite transformation, where the presence of potassium cation in the interlayer space catalyzes this mineral transformation (Cuadros et al. 1999).

The experimental crystal lattice structure of 2:1 dioctahedral phyllosilicates with high and low interlayer charge can be reproduced theoretically by means of total-energy calculations at the quantum-mechanical level. The pyrophyllite, beidellite, montmorillonite, and other different smectites and illites can be modeled by means of this methodology that can be extended

to the study of muscovite, margarite, and other micas and trioctahedral clays that have similar crystal structures. The most peculiar characteristic of these phyllosilicates is the interlayer space where the atomic interactions are much weaker than those in the crystal lattice. The quantum-mechanical method presented in this work is a useful tool to reproduce this interlayer space with the presence of interlayer cations. This fact is important to the extension of the application of this methodology to the study of geochemical processes such as mineral transformation, intercalations, dissolutions, and reactivity.

Effect of cation distribution

Different octahedral cation distributions have been studied in our calculations (Table 4). Samples S9 and S15 with an octahedral composition of Al_2Mg_2 can have different possible configurations. We have selected four distribution models that represent the main short-range ordering patterns for this composition (Fig. 2). Model I has no MgMg pair, and the Mg cations will see each other as a second neighbors (Fig. 2a). Model II represents a distribution where apparently the Mg cations are maximally separated within the unit cell. However, considering the whole octahedral sheet, this distribution implies the existence of MgMg pairs and some OH-bridging groups are between Mg cations [MgO(H)Mg] (Fig. 2b). Models III and IV represent the formation of MgMg pairs within the unit cell. Model III represent chains of Mg cations (Fig. 2c) and the OH-bridging groups are between Mg and Al cations [MgO(H)Al]. In model IV these groups are MgO(H)Mg (Fig. 2d). Considering the whole octahedral sheet as a supercell, models II and IV are identical.

For the Al_2Mg_2 octahedral composition, different interlayer cations were studied (K^+ in S9 and Ca^{2+} in S15). In each case, different distributions of octahedral cations were calculated following the models defined above. The total energy and main geometrical features were compared for each case and composition (Table 4). In both systems, the most stable distribution

TABLE 4. Structural parameters of models of illite-smectite with different cation distribution (lengths in Å and angles in degrees)

Sample*	S9a	S9b	S9c	S9d	S15a	S15b	S15c	S15d	S8a	S8b
ΔE (eV)	0.0†	0.634†	0.481†	0.353†	0.0‡	0.011‡	0.38‡	0.39‡	0.0§	0.11§
a	5.16	5.12	5.12	5.13	5.15	5.11	5.12	5.14	5.12	5.10
b	9.08	9.10	9.09	9.12	9.03	9.09	9.03	9.05	8.98	8.96
c	10.09	10.13	10.08	10.14	9.94	9.99	9.97	9.89	9.95	9.97
β	100.9	100.7	100.4	101.3	101.0	101.7	100.9	100.9	101.9	101.8
V (Å³)	462.4	464.0	461.6	465.3	453.5	454.2	453.3	451.8	447.4	446.0
T. th. ‖	2.32	2.30	2.31	2.26	2.31	2.23	2.30	2.30	2.24	2.24
Oc. th. ‖	2.19	2.24	2.21	2.20	2.18	2.18	2.19	2.18	2.13	2.13
Int. th. ‖	3.04	3.11	3.08	3.22	2.96	3.14	3.00	2.93	3.13	3.15
ΔZ#	0.15	0.17	0.10	0.20	0.19	0.22	0.15	0.15	0.22	0.22
τ#	112.4	113.4	113.0	113.1	113.5	113.0	113.0	112.5	110.8	110.6
ψ#	57.2	56.3	57.7	56.8	56.8	57.0	57.5	57.2	56.9	56.9
O-H #	0.981	0.984	0.982	0.977	0.981	0.983	0.982	0.978	0.992	0.986
T-O #	1.63	1.64	1.63	1.63	1.63	1.63	1.62	1.63	1.67	1.67
M-O #	2.02	2.02	2.07	2.01	1.99	2.00	2.04	2.01	1.95	1.95
M-OH #	1.97	1.92	1.97	2.04	1.96	1.92	1.96	2.00	1.89	1.92

* Models of cation distribution of octahedral cation in ilite-smectites S9, S15 and S8 (Fig. 2): S9a, S15a, and S8b = model I; S9b, and S15b = model II; S9c, and S15c = model III; S9d, S15d, and S8a = model IV.
† Respect to S9a = −11.597,879 eV.
‡ Respect to S15a = −11.612,187 eV.
§ Respect to S8a = −13.048,358 eV.
‖ T. th. = tetrahedral sheet thickness, O. th. = octahedral sheet thickness, Int. th. = interlayer thickness.
Mean values, ΔZ = corrugation effect of basal oxygen surfaces, τ = the O_{basal}-T-O_{apical} bond angle, ψ = octahedral flattening angle cos ψ = O. th. / 2(M-O), T is the cation of the tetrahedral sheet, M is the cation of the octahedral sheet.
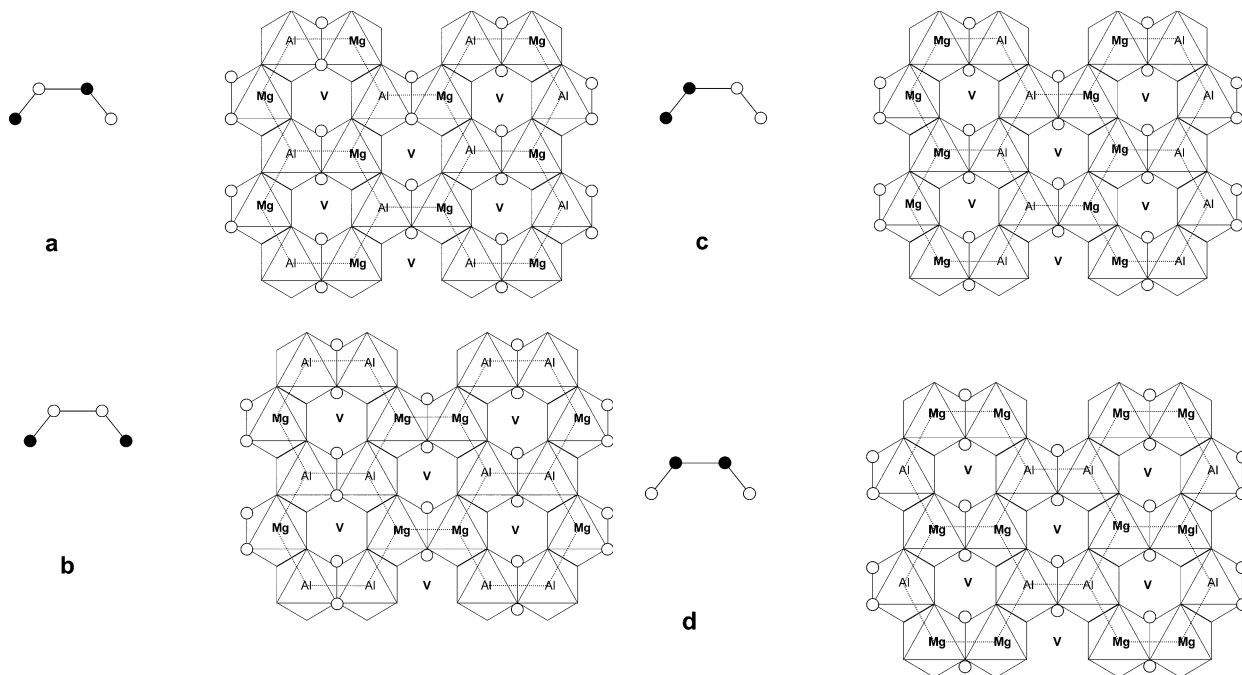

FIGURE 2. Cation distribution models for the octahedral sheet of 2:1 phyllosilicates, in a unit cell and in the crystal lattice. Models I (**a**), II (**b**), III (**c**), and IV (**d**).

corresponds to model I, where no MgMg pair is present (S9a and S15a). Experimental studies of cation ordering in smectites and illites gave the same result in that, no MgMg pair was found (Cuadros et al. 1999; Sainz-Diaz et al. 2001a). For $Al_2(Fe^{3+})_2$ octahedral composition (S8), the most stable distribution corresponds to model IV (Table 4), where the Fe cations form FeFe pairs (S8a). This is also consistent with experimental results for smectites and illites, where the Fe is mainly clustered in a short-range ordering pattern (Cuadros et al. 1999; Sainz-Díaz et al. 2001a). In Figure 3, some experimental cation dis-

tributions of the octahedral sheet of a natural bentonite mixed-layer illite-smectite [octahedral composition: $(Al_{3.17}Fe^{3+}_{0.24}Mg_{0.64})$ per unit cell] are shown. A disordered random cation distribution in this sample with a relatively high Mg content and a low Fe content will show some MgMg pairs and a negligible number of FeFe pairs (Fig. 3a). However, experimental studies by means of FT-IR, ^{27}Al NMR and inverse Monte Carlo simulations on this mineral (Fig. 3b) showed that Mg is dispersed and trends to form superstructures like model I presented in this paper. On the contrary, the Fe atoms tend to cluster, dramati-
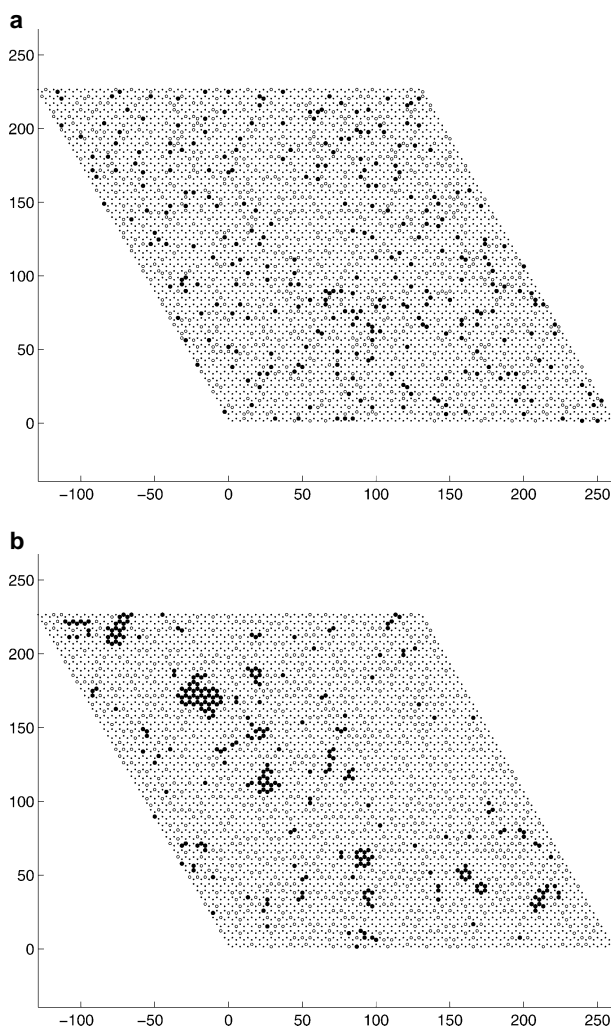
a

b

FIGURE 3. Representations of cation distributions of the octahedral sheet for a natural bentonite mixed-layer illite-smectite $[(Al_{3.17}Fe^{3+}_{0.24}Mg_{0.64})$ per unit cell, values for the X and Y parameters are in Å]: (**a**) disordered random distribution, and (**b**) experimental distribution. Al (·), Fe (●), Mg (o).

cally increasing the number of FeFe pairs as found in our calculations. In addition, our calculations match the experimental cation distribution of Mg and Fe along the octahedral sheet of clays. The dispersion trend of Mg and the clustering trend of Fe cations in the octahedral sheet of clay are well reproduced theoretically.

The effect of the octahedral cation distribution on the crystallographic parameters is not very significant. In S8a the OH groups are joined to two Fe cations whereas in S8b the hydroxy groups are joined to only one Fe cation. In S8a the M-OH bond length is smaller than in **S8b**. This fact can be due to the higher covalent character of the Fe-O bond (a higher overlapping between the oxygen orbital and the Fe d orbital) than the other M-O bonds in the octahedral sheet, increasing the electron density when the Fe cations are clustered (Sherman

1985; Sainz-Diaz et al. 2000). In addition, the O-H bond is longer in S8a than in S8b. A longer O-H bond length is related to a lower $\nu(OH)$ frequency. This fact is consistent with the experimental phenomenon, where the $\nu(OH)$ frequency is lower for Fe(OH)Fe groups (as in S8a) than for Fe(OH)Al groups (as in S8b) (Besson and Drits 1997). Therefore, our theoretical study of the cation pair substitution effect on the OH frequency agrees with experimental results. Further calculations will be performed on larger supercells of these minerals to obtain a better description of longer-range effects in these systems.

REFERENCES CITED

Artacho, E., Sánchez-Portal, D., Ordejón, P., García, A., and Soler, J.M. (1999). Linear-scaling ab-initio calculations for large and complex systems. Physic Status Solidi, 215, 809–817.
Bachelet, G.B. and Schluter, M. (1982) Relativistic norm-conserving pseudopotentials. Physical Review B, 25, 2103–2108.
Besson, G. and Drits, V.A. (1997) Refined relationship between chemical composition of dioctahedral fine-grained micaceous minerals and their infrared spectra within the OH stretching region. Clays and Clay Minerals, 45, 170–183.
Bosenick, A., Dove, M.T., Myers, E.R., Palin, E., Sainz-Díaz, C.I., Guiton, B., Warren, M.C., Craig, M.S., and Redfern, S.A.T. (2001) Computational methods for the study of energies of cation distributions: applications to cation-ordering phase transitions and solid solutions. Mineralogical Magazine, 65, 197–224.
Bridgeman, C.H., Buckingham, A.D., Skipper, N.T., and Payne, M.C. (1996) Ab initio total energy study of uncharged 2:1 clays and their interaction with water. Molecular Physics, 89, 879–888.
Brown, G. and Brindley, G.W. (1980) X-ray diffraction procedures for clay mineral identification. In: Brindley GW, and Brown G. (Eds.) Crystal structures of clay minerals and their X-ray identification. Mineralogical Society, London, p. 305–360.
Chatterjee, A., Iwasaki, T., and Ebina, T. (2000) A novel method to correlate layer charge and the catalytic activity of 2:1 dioctahedral smectite clays in terms of binding the interlayer cation surrounded by monohydrate. Journal of Physical Chemistry A, 104, 8216–8223.
Collins, D.R. and Catlow, C.R. (1992) Computer simulations of structures and cohesive properties of micas. American Mineralogist, 77, 1172–1181.
Cuadros, J., Sainz-Díaz, C.I., Ramírez, R., and Hernández-Laguna, A. (1999) Analysis of Fe segregation in the octahedral sheet of bentonitic illite-smectite by means of FT-IR, ^{27}Al MAS NMR and reverse Monte Carlo simulations. American Journal of Science, 299, 289–308.
Giese, R.F. Jr. (1979) Hydroxyl orientations in 2:1 phyllosilicates. Clays and Clay Minerals, 27, 213–223.
Guggenheim, S., Chang, Y.-H., and Koster van Groos, A.F. (1987) Muscovite dehydroxylation, high temperature studies. American Mineralogist, 72, 537–550.
Hebenstreit, J. and Scheffler, M. (1992) Self-consistent pseudopotential calculations for sodium adsorption on GaAs(110). Physical Reviews B, 46, 10134–10140.
Herrero, C.P. and Sanz, J. (1991) Short-range order of the Si,Al distribution in layer silicates. Journal of Physical Chemistry of Solids, 52, 1129–1135.
Hobbs, J.D., Cygan, R.T., Nagy, K.L., Schultz, P.A., and Sears, M.P. (1997) All-atom ab initio energy minimization of the kaolinite crystal structure. American Mineralogist, 82, 657–662.
Junquera, J., Paz, O., Sánchez-Portal, D., and Artacho, E. (2001) Numerical atomic orbitals for linear-scaling calculations. Physical Review B, 64, 235111–1.
Karaborni, S., Smit, B., Heidug, W., Urai, J., and Van Oort, E. (1996) The swelling of clays: Molecular simulations of the hydration of montmorillonite. Science, 271, 1102–1104.
Kleinman, L. and Bylander, D.M. (1982) Efficacious form for model pseudopotentials. Physical Review Letters, 48, 1425–1428.
Kubicki, J.D. and Apitz, S.E. (1998). Molecular cluster models of aluminum oxide and aluminum hydroxide surfaces. American Mineralogist, 83, 1054–1066.
Kubicki, J.D., Blake, G.A., and Apitz, S.E. (1996) Ab initio calculations on alumi-nosilicate Q^3 species: Implications for atomic structures of mineral surfaces and dissolution mechanisms of feldspars. American Mineralogist, 81, 789–799.
Lasaga, A.C. (1995) Fundamental approaches in describing mineral dissolution and

precipitation rates. In A.F. White and S.L. Brantley, Eds., Chemical weathering rates of silicate minerals, 31, 23–86. Reviews in Mineralogy, Mineralogical Society of America, Washington, D.C.

Lee, C., Vanderbilt, D., Laasonen, K., Car, R., and Parrinello, M. (1993) Ab initio studies on the structural and dynamical properties of ice. Physical Review B, 47, 4863–4872.

Lee, J.H. and Guggenheim, S. (1981) Single crystal X-ray refinement of pyrophyllite-1*Tc*. American Mineralogist, 66, 350–357.

Louie, S.G., Froyen, S., and Cohen, M.L. (1982) Nonlinear ionic pseudopotentials in spin-density-functional calculations. Physical Review B, 26, 1738–1742.

Ordejón, P., Artacho, E., and Soler, J.M. (1996) Mixed approach to incorporate self-consistency into order-n LCAO methods. Material Research Society Symposium Proceedings, 408, 85–90.

Palin, E.J., Dove, M.T., Redfern, S.A.T., Bosenick, A, Sainz-Díaz, C.I., and Warren, M.C. (2001) Computational study of tetrahedral Al-Si ordering in muscovite. Physics and Chemistry of Minerals, 28, 534–544.

Payne, M.C., Teter, M.P., Allan, D.C., Arias, T.A., and Joannopoulos, J.D. (1992) Iterative minimization techniques for ab initio total-energy calculations: molecular dynamics and conjugate gradients. Reviews in Modern Physics, 64, 1045–1097.

Perdew, J.P., Burke, K., and Ernzerhof, M. (1996) Generalized gradient approximation made simple. Physical Review Letters, 77, 3865–3868.

Sainz-Díaz, C.I., Timón, V., Botella, V., and Hernández-Laguna, A. (2000) Isomorphous substitution effect on the vibration frequencies of hydroxyl groups in molecular cluster models of the clay octahedral sheet. American Mineralogist, 85, 1038–1045.

Sainz-Díaz, C.I., Cuadros, J., and Hernández-Laguna, A. (2001a) Analysis of cation distribution in the octahedral sheet of dioctahedral 2:1 phyllosilicates by using inverse Monte Carlo methods. Physics and Chemistry of Minerals, 28, 445–454.

Sainz-Díaz, C.I., Hernández-Laguna, A., and Dove, M.T. (2001b) Modelling of dioctahedral 2:1 phyllosilicates by means of transferable empirical potentials. Physics and Chemistry of Minerals, 28, 130–141.

Sánchez-Portal, D., Ordejón, P., Artacho, E., and Soler, J.M. (1997) Density-func-

tional method for very large systems with LCAO basis sets. International Journal of Quantum Chemistry, 65, 453–461.

Sauer, J., Ugliengo, P., Garrone, E., and Saunders, V.R. (1994) Theoretical study of van der Waals complexes at surface sites in comparison with the experiment. Chemical Reviews, 94, 2095–2160.

Sherman, D.M. (1985) The electronic structures of Fe^{3+} co-ordination sites in iron oxides. Application to spectra, bonding and magnetism. Physics and Chemistry of Minerals, 12, 161–175.

———(1991) Hartree-Fock band structure, equation of state, and pressure-induced hydrogen bonding in brucite, $Mg(OH)_2$. American Mineralogist, 76, 1769–1772.

Smrcok, L. and Benco, L. (1996) Ab initio periodic Hartree-Fock study of lizardite 1T. American Mineralogist, 81, 1405–1412.

Stich, I., Parrinello M., and Holender, J.M. (1996) Dynamics, spin fluctuations, and bonding in liquid silicon. Physical Review Letters, 76, 2077–2080.

Teppen, B.J., Rasmussen, K., Bertsch, P.M., Miller, D.M., and Schafer, L. (1997) Molecular dynamics modelling of clay minerals. 1. Gibbsite, Kaolinite, Pyrophyllite, and Beidellite. Journal of Physical Chemistry B, 101, 1579–1587.

Tsipursky, S.I. and Drits, V.A. (1984) The distribution of octahedral cations in the 2:1 layers of dioctahedral smectites studied by oblique-texture electron diffraction. Clay Minerals, 19, 177–193.

Troullier, N. and Martins, J.L. (1991) Efficient pseudopotentials in spin-density-functional calculations. Physical Review B, 43, 1993–2006.

Wardle, R. and Brindley, G.W. (1972) The crystal structures of pyrophyllite-1Tc, and its dehydroxylate. American Mineralogist, 57, 732–750.

Winkler, B., Milman, V., and Payne, M.C. (1995) *Ab initio* total energy studies of minerals using density functional theory and the local density approximation. Mineralogical Magazine, 59, 589–596.

Winkler, B., Milman, V., Hytha, M., Pickard, C. J., and Warren, M. (2001) Theoretical investigation of bonding in diaspore. European Journal of Mineralogy, 13, 343–349.